Pre-Print Submitted to Journal of Thermal Science

Accuracy details in realistic CFD modeling of an industrial centrifugal pump in direct and reverse modes

J.C. Páscoa[1], F. J. Silva[1], J.S. Pinheiro[2] and D.J. Martins[2]

1. Department of Electromechanical Engineering, Center for Aerospace Sciences and Technology, University of Beira Interior, R. Mq.s D´Ávila e Bolama, 6201-001 Covilhã, Portugal
2. EFAFLU Bombas e Ventiladores S.A., R. S. Brás, 269, Apartado 23, 4494-909 Póvoa do Varzim, Portugal

Numerical computation of the flowfield inside a pump is herein used as a numerical laboratory, subject to the limitations of modeling assumptions and to experimental verification. A numerical computation of the flow inside a real industrial centrifugal pump is performed that includes a very sophisticated geometry. Conversely to other computations, in this test case no simplification of the geometry was introduced. Numerical computations are obtained using Spalart-Allmaras turbulence model. A detailed analysis of the turbulent flowstructure is performed for the design point and two off design conditions. Additional computations were performed in order to compare the numerical and experimental pump characteristics; these were obtained under normalized testing conditions. Further computations are presented for the pump working in reverse turbine mode (PAT). Detailed analyses of the flow allow a comparison of the internal flow losses when the pump is operating in direct and reverse mode. This is also useful to help in the selection of an adequate pump geometry that can work in both modes with best efficiency.

Keywords: centrifugal pump, impeller, turbulence modeling, Spalart-Allmaras, PAT

Introduction

The inherent unsteadiness, the cavitation problems, secondary flows and turbulent structures make the modeling of the flow inside a pump a challenging task. In the past 50 years a combination of model testing, empirical correlations and inspired engineering resulted in pumps having excellent performances [1]. Yet, in order to achieve better designs, particularly at off-design conditions, it is nowadays clear that a detailed knowledge of internal flow is required. Attaining this knowledge using experimental techniques implies the use of Particle Image Velocimetry, or at best laser Doppler [2, 3]. These methods conduct to overwhelming problems associated to the optical access to the internal pump flow, besides of being extremely expensive and time consuming. When subjected to appropriate critical insight Computational Fluid Dynamics (CFD) resulted in an approach that can successfully contribute to the improved design of hydraulic pumps [4].

The use of CFD tools to design these complex machines has only been made possible due to the increasing availability of computing resources. These evolved side-by-side with an increase in accuracy of numerical methods, and CFD shifted from a pure academic research tool into the competitive industrial companies design offices [5, 6, 7, 8]. A main breakthrough occurred in the late 90's, when numerical codes developed their assump-

Received: June 2010
José C. Páscoa: Ph.D., Professor Auxiliar (pascoa@ubi.pt)

tions from a pure inviscid physical model into viscous turbulent models. However, and due to the increased computer power required by these methods, only 2D or quasi-3D computations for simplified isolated pump components were possible [9, 10]. Even so, much of this work in isolated components allowed an increase in efficiency of pump elements, such as the impeller, volutes and guide vanes. Only in recent years it became possible to compute a full 3D flowfield inside realistic pump geometries [11]. This is an extremely valuable tool to take into account the internal component interactions. Nevertheless, and to become useful, the results of these computations require that the designers have a deep knowledge of flow physics and of the underlying modeling limitations. Even nowadays, current state-of-the-art modeling can not cope with detailed features in a global way. In case of using numerical and optimization methods to automate design this is even worse [12]. Detailed features such as wear-ring seals are usually coupled using an analytical-numerical approach [13]. The weaknesses associated to the empirical nature of turbulence models implies that numerical results must recursively be benchmarked with experimental testing [14].

In numerical modeling of pump flows there are additional complexities not present in pure stationary frame of reference flows. The interaction between stator and rotor must be tackled, and this is usually done using three different approaches; frozen-rotor, mixing-plane, and pure unsteady computation. The most demanding in computer power, and best accurate, is the full unsteady computation. In the frozen-rotor approach a quasi-steady computation of the flow is made, and in the mixing-plane approach a pure steady computation is done. The reference to unsteadiness refers to the way in which we solve the stator-rotor interaction, as even for a mixing-plane approach an unsteady computation of the internal flow field is possible, albeit in this later case we loose the unsteady information in the vicinity of the mixing-plane. In the frozen rotor the grid is frozen in time, and this is best accurate for axial flow pumps due to circumferential periodicity of the geometry. With the mixing-plane approach the computation is performed by averaging the flux variables in the planes defining the stator and rotor fluids. This allows computing the flow using only one blade, thus reducing the grid node count. A faster computation can then be performed for the cases in which this method does not exhibit convergence problems. These problems usually occur due to a very small gap between stator and rotor and due to unsteadiness of the flow impinging on the mixing-plane. This can be caused by a thick trailing edge on an inlet stator blade, as happened in our computations. Another source of problems is in the pump tongue zone. We were not able to achieve a fully converged mixing-plane solution due to the very compact nature of our centrifugal pump. As very compact pumps are increasingly common, the mixing-plane approach becomes infeasible for most commercial pump geometries. Yet, it is advisable to use the mixing-plane model in cases the gap is enough to sustain a good convergence of the numerical code, as is the case for high volute-rotor ratios. Alternatively the unsteady computation involves a sliding of the rotor mesh in the continuity interfaces with the stator, between the moving and static fluid. In that case a fully converged solution must be obtained for each time-step. The time-step must be sufficiently small to achieve a good resolution of unsteadiness, and this result in high computing power requirements. For the present computations we have applied a frozen-rotor approach, due to the existence of a small gap between rotor and tongue, and in order to reduce the burden of performing unsteady computations.

One fundamental factor that introduces a weakness in CFD pump design, especially for routinely design purposes, is related to turbulence modeling. The computations must be performed by means of the Reynolds Averaged Navier-Stokes (RANS) equations with an appropriate turbulence model. Direct Numerical Simulation is out of range due to the high computer power needed, and Large Eddy Simulation is currently only feasible for simplified pump elements. As implied, by time averaging the equations we must define a way to compute the Reynolds stresses. Actually, instead of solving for the Reynolds stresses an eddy viscosity approach is applied. There is a wide range of turbulence models developed; each has its own weaknesses and virtues. Most of the best performing are implemented in Fluent commercial code, as is the case of k–ε, k–ω and Spalart-Allmaras. For our computations we have used k–ε and Spalart-Allmaras. Actually, this later resulted in more accurate results computed for the pump when compared with experiments. Spalart-Allmaras is a low-Re turbulence model and therefore can be used without wall functions. For the case of k–ε, as it is a high-Re turbulence closure, a near wall result must be obtained using wall functions. These functions are of empirical nature and allow predicting the flow in the near wall region using very crude meshes. Using Spalart-Allmaras without wall functions implies that the first computational cell above the wall must lie in the laminar sub-layer, with y+=1. Using wall functions, even with the low-Re Spalart-Allmaras model, implies that the first cell above the wall can be defined in the logarithmic layer, thus resulting in a reduced grid count for the boundary layer flow. On a typical mesh used to integrate to the wall it would be needed 40 computing cells to resolve the boundary layer, this will reduce to 15 when applying wall functions for a y^+ near 100 [15]. Yet, the y^+ can reach the validity limit of 300 and thus the reduction in grid cell number can be even greater. We should also refer that the

computational efficiency will be further increased due to a reduction of the aspect-ratio; typically wall resolving grids have high aspect ratio that compromise convergence due to round-off errors. The high computing cost of resolving the full wall boundary, without wall functions, is contra productive for daily pump design practice. On course of this work several meshes were created in order to ensure that the grid is in the validity range of the wall functions, y^+ between 30 and 300, see [16].

In this work we present a detailed analysis of the flow inside an industrial centrifugal pump manufactured by Efaflu – Bombas e Ventiladores S.A. [1]. The proposed work resulted from three main challenges. First, how to most accurately model the geometry using an adequate mesh. Even the most recent works presented in the literature resort to simplifications applied into the computed geometry [17, 18, 19]. In the present case the only simplification was the non-inclusion of wear-ring seals. A detailed description is presented regarding the problems, and proposed solutions, obtained on course of this work. This is presented in second Section. The second challenge is to know how accurately the pump can be modeled using the frozen-rotor approach and associated turbulence closures. We have compared the numerical results with the experiments obtained for the same pump under normalized conditions. A detailed analysis for design and off-design conditions is given in the third Section. This resulted in suggestions for the redesign of the pump. A final challenge is the application of the pump working as turbine. A detailed analysis of the efficiency, internal flow losses and axial forces is presented and compared to direct (pumping) mode in last Section.

Numerical Model For The Benchmark Test Case

Herein we describe the NNJ pump used in the computations. A detailed description of the mesh generation procedure is given in order to take into account the very fine details of the pump. The pump was subject to experimental testing at the normalized pump test bench of Efaflu - Bombas e Ventiladores S.A.

NNJ 125-250 centrifugal pump geometry and grid generation

One of the goals of the present work is to achieve a very precise definition of the geometry by means of the computational mesh. In our case the mesh was created from a 3D CAD file given by the manufacturer, see Fig.1. This ensures that when creating the mesh all the detailed features of the pump are incorporated. Even if the mesh generator within Fluent enables us to create an almost automatic mesh, this was not the procedure followed. A very strict procedure was performed, in which the mesh was subdivided into several blocks, and a very detailed

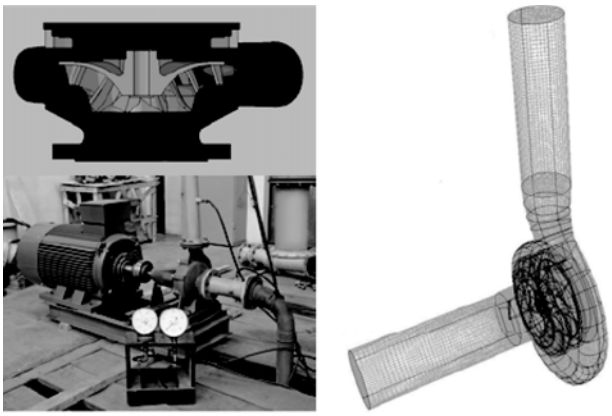

Fig. 1 The 130 kW NNJ 125-250 centrifugal pump: a) A section view of the pump and partial view of the experimental facility at Efaflu S.A., typical normalized measurements are for flowrate and manometric pressure at pump inlet and outlet. b) A global view of the mesh created to perform the computations with 2 134 777 volumes.

analysis of the mesh quality was made for each block.

The NNJ series is an industry normalized class of pumps. This centrifugal pump is very complex as it features an inlet guide vane at rotor entrance, and further it includes in the backrotor six structural vanes; see Fig.1-a). The purpose of the backrotor vanes is to perform equilibrium of the axial force in the shaft due to Bernoulli effect caused by its rotating core fluid. Additionally we can see a partial view of the experimental testing facility at Efaflu - Bombas e Ventiladores S. A. Normalized procedures are conducted at this testing station in order to obtain the pump characteristics. A global view of one of the generated meshes can be appreciated in Fig.1-b), it comprises 2 134 777 volumes.

The pump rotor is of the shrouded type; it has a nominal diameter of 265 mm and comprises 8 blades. The suction duct has a diameter of 148.50 mm that reduces to 125 mm in the pressure duct. Catalogue data for this pump series is available from [1].

The grid is composed by 12 geometrical blocks, see Tab. 1. Some of the most important blocks are visible in Fig. 2. For each of the blocks we construct interfaces that allow the transfer of kinematic variables between the bordering fluid blocks. Besides the geometrical blocks we also define two fluid blocks, these comprise the stationary and rotating fluid. A rotating fluid block is defined in the rotor and a second rotating fluid block is also defined for the rotor backward vanes. The remaining fluid is considered in a stationary reference frame. In order to obtain a good mesh quality we have performed detailed aspect-ratio and equi-angle adjustments by redistributing the nodes in all over the grid blocks. As an

Table 1 Explanation of the grid blocks created to define the pump, including a description of the imposed boundary conditions and of the numerical model.

Parameter	Numerical grid
Domain of simulation	Block A+Block B+Block C(impeller-8 blade passages)+Block D+Block E+Block F+Block G+Block H+Block I+Block J(volute casing)+ Block k+Block L
Extended inlet duct grid	Unstructured 135 129 cells (tet+pyr)
Extended outlet duct grid	Unstructured 87 461 cells (tet+pyr)
Impeller frid	Unstructured 881 138 cells (tet+pyr)
Volute casing grid	Unstructured 407 017 cells (tet+pyr)
Block D	Structured 9 555 cells
Boundary conditions and numerical methods	
Inlet	Total pressure=0 Pa
Outlet	Gauge pressure=735 671.5 Pa
Interface impeller/volute	Frozen Rotor
Turbulence model	Spalart-Allmaras
Spatial discretization	Second order

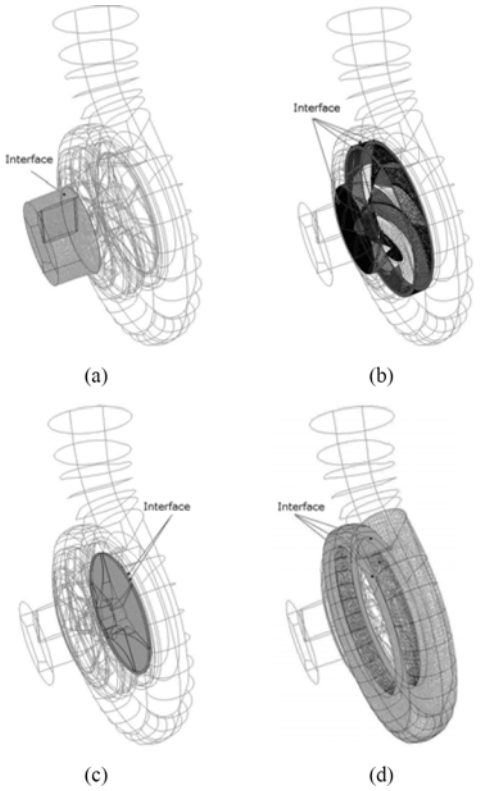

Fig. 2 The grid used to model the flow inside the centrifugal pump comprises 12 blocks. The most significant blocks are: (a) The inlet guide vane block that achieves a detailed modeling of the zone between the suction block and the rotor block. (b) A block for the shrouded rotor that was created using a pure unstructured grid due to the complexity of the geometry. (c) A second rotor block associated to the moving fluid in the back-rotor vanes. (d) The volute casing block that is defined in a stationary reference frame.

example, in Fig. 3 we can see a redesign of the mesh for the inlet guide vane. This was made in order to achieve a reduction in skewness. Initially the mesh was completely structured, as this is beneficial in terms of resolving the boundary layers. Unfortunately this resulted in a bad quality mesh and thus we have resorted to a mixed structured-unstructured mesh. The grid aspect-ratio parameter is extremely important to achieve a good convergence rate; actually in worst cases it can actually make convergence almost impossible. It is useless to have a nice structured mesh in the boundary layer that cannot converge at all.

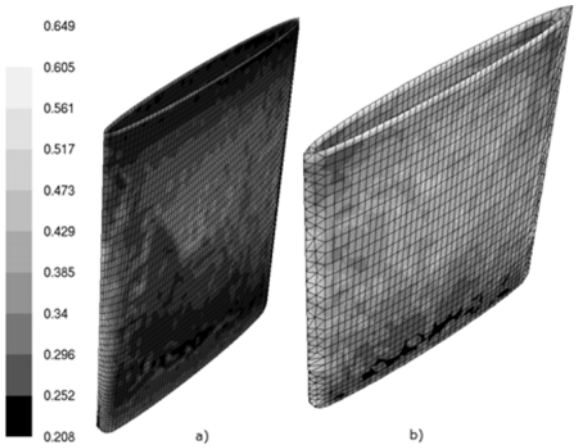

Fig. 3 Evaluations of the skewness parameter in mesh of the inlet guide vane. (a) Initially the cells were all of the structured type. (b) In a second step we have recreated the mesh using structured and unstructured meshes. A major reduction in skewness was achieved.

Numerical model used to compute the flow

The numerical computations were performed using Fluent 6.3 commercial CFD code. The flow is modeled using the RANS equations in 3D, including the centrifugal force effects in rotor. The fluid is considered incompressible. The computation is performed by marching to the steady-state using a pseudo-unsteady formulation. This pseudo-unsteady approach enables a faster convergence to steady state, but the intermediate solutions have no physical significance. As we were mainly interested in a steady-state solution we followed this approach to achieve faster convergence. Solutions were attempted using two turbulence models, namely k–ε and Spalart-Allmaras.

With preliminary computations we established that the Spalart-Allmaras was the method that best approached the experimental results. Therefore this was the chosen method to compute the remaining solutions presented in this work. Albeit Spalart-Allmaras is a low-Re turbulence model, and can be used to compute near wall flows, for reasons of computational efficiency we have applied wall functions. A second-order discretization in space was

used to obtain every final result, albeit computations started always in first order to achieve a main bulk initial flow. This resulted in faster solutions than the ones obtained if we started the computations initially from first order. The PISO algorithm was used to march in pseudo-time. This algorithm was used in a coupled solution procedure for the system of equations. We realized that this coupling was of foremost importance to achieve a second-order convergence with this kind of very complex grid. Even with all the care we have taken to create the mesh, there were some remaining lower quality areas that hindered the convergence of initial computations. The results herein present were obtained using a frozen rotor approach to take into account the stator-rotor interaction. Some initial computations were attempted using the mixing-plane assumption but were unsuccessful, as expected, in view of the high volute-rotor radius ratio. This happened in the tongue region, for the rotor, and also due to the inlet guide-vane that was too close to the inlet rotor interface.

Another important aspect of the implementation of the numerical model is the choice of boundary conditions. No slip and wall interface are normal conditions for the viscous walls and for the connection of the fluid between the moving and rotating frame of reference. A different question arises when we tackled the problem of the inlet and outlet boundaries. There are in the literature diverse type of boundary conditions that were considered for these boundaries [18, 20].

A vast majority of the results presented in the literature apply a mixed type condition, using static pressure at outlet and mass flow at inlet. This condition is very robust and allows a direct control on the inlet mass flow. Results have usually a fast convergence rate. Yet, this type of boundary condition is not a natural boundary condition due to the imposition of the mass flow. Unsteady effects present in the flowfield will have a tendency to being filtered, in spite of achieving convergence in poor quality meshes. A more natural condition is the imposition of a stagnation pressure at inlet and a static pressure at outlet, with the mass flow resulting from this imposed pressure difference. The use of this condition requires usually a good quality mesh, as the one we created for this work. Incidentally the inlet stagnation pressure can be referred to the pressure head $\Delta P=P_2-P_1$, and this allows a prediction of the computing point as compared to the pump characteristics. Further, a moving reference frame was applied to the rotating fluid and all the results were obtained for a nominal pump rotation of 2900 r/min.

Results Obtained for the Computation of the Flow

In this section we will present the numerical results obtained for the centrifugal pump in direct and reverse mode. Computations were performed for design and off-design conditions.

Investigation of the flow in the pump

In order to check the validity of the numerical model we have compared the numerical results with the experiments. These experiments were obtained in Efaflu S.A. testing station, seen in Fig1-a). The results from the experiments present a relative error below 2%. This is mainly pushed up by flowrate measurements, since the pressure measurements are much more precise. In Fig. 4 we present a direct comparison between the experimental and numerical characteristics. Numerical results are systematic below the experimental characteristic, around 5%.

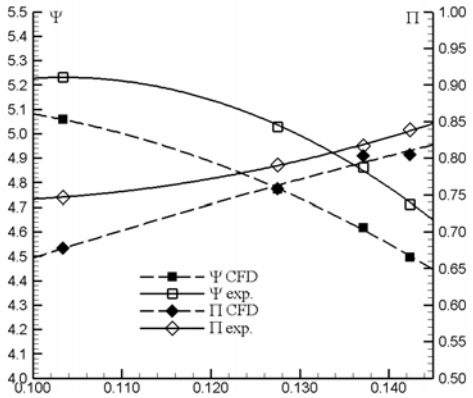

Fig. 4 Experimental validation of the numerical model for the centrifugal pump in direct mode. Comparison of head parameter $\Psi=gH/N^2D^2$ and power parameter $\pi_P=P/\rho N^3D^5$ as a function of flow parameter $\Phi=Q/ND^3$. Notice that this is a detailed view, due to a rearrange of the axis, that amplifies the discrepancies.

This is to be expected as we have used the frozen rotor model. In regards efficiency, numerical results give an efficiency of 77% and experiments provide 79%. A very small discrepancy indeed, below 2.5%. We have thus decided to investigate the effect of rotor position into the computed results.

In Fig. 5 we can see that diverse values for the flowrate are to be expected when we use the frozen rotor at a different position from the tongue. These corresponds to the different frozen-rotors computations.

The results of the computations taken at different blade-tongue positions can be seen in Fig.6. This demonstrates that the flowrate changes at the diverse positions. Accordingly, only a full unsteady computation can approach accurately the experimental results. Albeit these minor discrepancies between the CFD results obtained for each frozen rotor position and the experiments, with

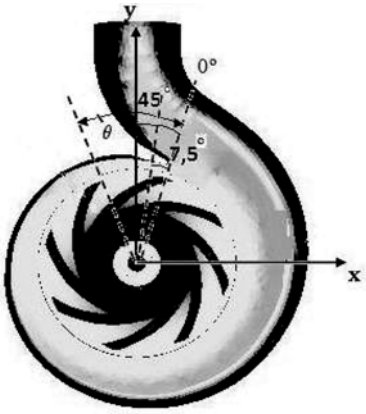

Fig. 5 Relative positions of one blade in relation to the volute, each corresponds to a frozen rotor computation.

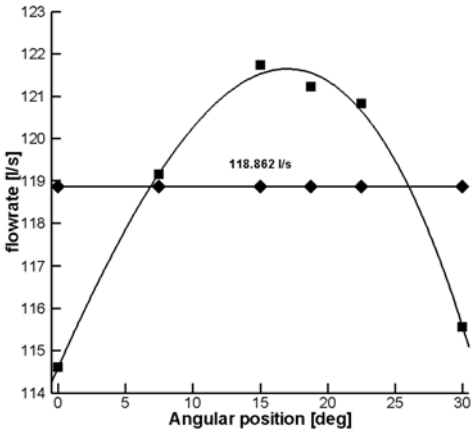

Fig. 6 Results obtained for different frozen rotor positions, it is evident that flowrate changes as a function of angular blade position, relative to tongue. The mean value is 118.862 l/s.

just one frozen rotor computation we have already results that can help in redesigning the pump.

The initial position seen in Fig. 5 refers to the initial position of the rotor used in the first computations. These results were obtained for the same pressure difference, and the flowrate evolves as a function of blade position. The peak maximum flowrate is attained for an angular position of around 16º. The pump has 8 blades and this corresponds to a step of 45º, this step was here further subdivided into 7.5º to make the computations.

We will now proceed to analyze in detail the internal flow of the pump, both for design and off-design conditions. In Tab. 2 we make a comparison between the experimental and numerical results at the design point (around 122.07 l/s) and also for values ranging from 99.42 to 130.20 liters per second.

In Fig. 7 we can have an insight on how the flow-structure changes as we move to upper and lower values of the flowrate design point. Interesting is here to note how has changed the pressure in the volute exit, as this regulates the maximum flowrate that can be achieved by the pump. However, in order to have a detailed knowledge of the flow inside the pump we must resort to the streamline pattern for the two off-design computations, see Fig. 8. It is interesting to observe the occurrence of a recirculation bubble for the computations at 1.047Qn. For the part load computations we do not observe this behavior.

Table 2 Comparison between the experimental results and the results obtained with the numerical model. Static pressure values are presented for a range of five working conditions.

Numerical			Experimental	
Q[l/s]	ΔP[Pa]	H[m]	DP[Pa]	H[m]
99.42	817 250.7	73.3	873 090.0	89.0
114.70	782 738.4	79.8	825 000.0	84.1
122.07	760 636.7	77.5	810 000.0	82.7
128.06	738 152.6	75.2	787 500.0	80.3
130.20	729 105.4	74.3	781 250.0	79.6

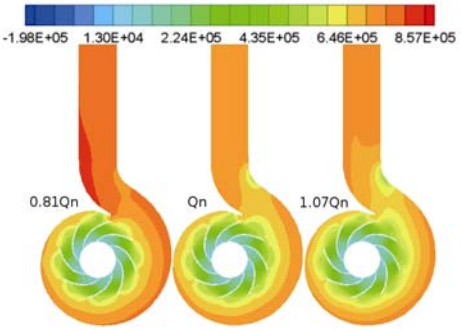

Fig. 7 Changes in static pressure field depict the flow structure due to off-design conditions, here Q_n~ 122 *l/s* for this pump. The results were obtained for a section of the pump at mid rotor height.

Numerical results for the pump working as turbine in reverse mode

In some circumstances centrifugal pumps have been proposed in the literature to operate in reverse pumping mode [21]. This is generally the case for pico-turbine sites, in which the development of small turbines for diverse working conditions is not economically feasible. Actually the price ratio between the small turbines and the Pump-As-Turbine (PAT) can attain values of 7 to 1. This certainly stimulates the application of PATs and also research on the flowfield inside these machines. In most cases the selection of a certain pump to work as PAT is made using empirical correlations, such as the ones given by Williams, in part because most of the pump manufacturers do not provide the experimental characteristics in reverse mode. However, by running our numerical model in these reverse operating conditions we can very easily analyze the performance of pumps operating as turbines.

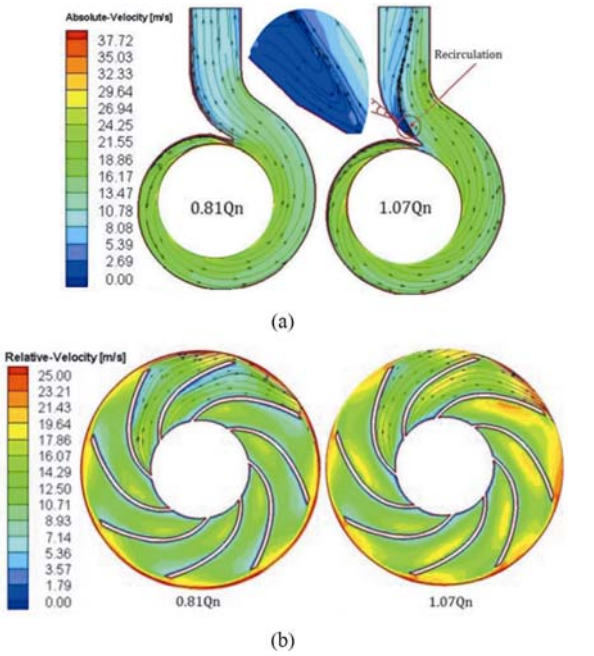

Fig. 8 Streamlines inside the pump for a section at mid rotor height: a) flow in the volute casing with a detailed view of a recirculating bubble. b) Flow in the rotor with the velocities represented in the relative frame of reference.

In our model we need to impose, as boundary condition, the head pressure ratio. This can be obtained by extrapolating the nominal design point, as a pump, to the nominal design point as a turbine, see Fig. 9. In order to start the computations we have used Williams[22] correlation to obtain the nominal values in turbine mode from nominal pump mode. In this case we need to know, besides the head and flowrate, the maximum efficiency of the pump. We have used our computed results for direct mode, thus $\eta_{max} = 77\%$.

$$Q_t = \frac{Q_{BEP}}{\eta_{\max}^{0.8}} = 151.61 \text{ l/s}, \; H_t = \frac{H_{BEP}}{\eta_{\max}^{1.2}} = 112.2 \text{ m}. \quad (1)$$

Only minor modifications must be made to the numerical model of the turbine. In this case we have changed the static pressure ratio, by imposing the value given by the previous equations, and also the rotating direction of the pump was reversed. The results obtained using our CFD model for turbine mode of operation were Q= 145.5 *l/s* and H=113.8 *m* (1 116 960.2 Pa). It is interesting to note that operation in pump mode results in quite different pattern of losses, as can be seen in Fig. 9-b) and -c).

Another question arose that is related to know if the pump working in reverse mode can have some problems related to axial shaft forces, as we have increased the head, see Eq. (1). The new values of pressure ratio are much higher than the ones attained in pumping mode. So,

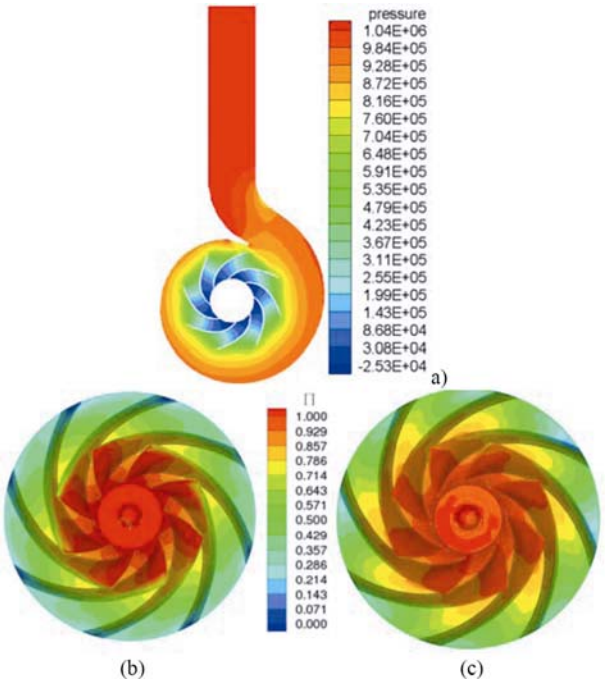

Fig. 9 Results obtained for the (PAT) pump-as-turbine: a) Static pressure distribution in turbine mode for a section at mid rotor height. b) Stagnation pressure loss when operating in pump mode at nominal conditions. c) Stagnation pressure loss when operating in pump-as-turbine for the turbine nominal conditions. Values are normalized by rotor inlet stagnation pressure $\Pi = 1 - p_{tot}/p_{tot.in}$.

it is to be expected that some problems can arise due to axial load in the shaft bearings. We have computed the axial force in direct and inverse mode (pump Q=123.33 *l/s* and H=77.20 *m*; PAT Q=151.61 *l/s* and H=112.2 *m*). In pump mode we have obtained an axial force of 587.86 *N* and in reverse mode *205.85 N*. In order to being able to compare these two values we must perform a nondimensionalization using $C_{F_z} = F_z/(\Delta P \times A_R)$, being ΔP the pressure head in the corresponding mode of operation. We have obtained an axial shaft force 3.7 times higher in pump mode as compared to reverse mode. This means that the PAT can cope with the shaft axial force. However, in case the PAT is to be expected to operate at higher velocities than in pump mode, then, other problems can arise.

For the centrifugal pump we have noticed the existence of six structural radial vanes in the back-rotor. These have the effect of reducing the pressure from P_1 to P_2. see Fig.10. This happens in the small space between the back of the rotor and the pump. Only by modeling this detailed pump feature we could compute the real axial force. In this area, the 6 vanes increase the kinetic energy of the local fluid and this contributes to a decrease

in pressure. Another question is related to the changes occurring in the efficiency for reverse and direct operating mode. The efficiency computed in reverse mode (η=72.6%) is lower than when working in direct mode (η=77%).

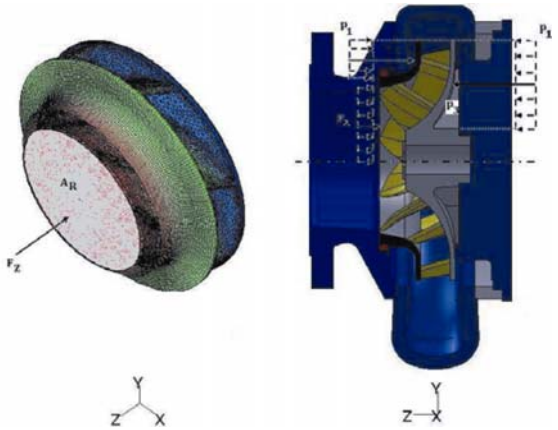

Fig. 10 Axial force acting in pump rotor, this can be computed from CFD results for pump and turbine modes. Here we can see an idealized pressure distribution for the pump rotor.

Conclusions

The work presented a detailed overview of the numerical modeling of an industrial centrifugal pump. A very careful generation of the grid allowed us to compute the flow both in direct and inverse mode. This careful mesh generation procedure was very important in order to achieve a second order convergence of the solution. Even if first order results can be useful in a global view, only second order results can allows us to make a detailed analysis of the internal flow with an appropriate confidence level.

In order to ensure the validity of the numerical model the numerical computations were compared to experiments. Results present a very good accuracy in view of the taken assumptions. By using a frozen rotor approach we have checked if, and how, did the flowrate changed as a function of the relative position of the blade and tongue. We concluded that the flowrate changed as a function of the relative rotor position. This result was only possible to be obtained because we have used pressure boundary conditions, for the inlet and outlet boundaries of the pump. A detailed analysis of the flow pattern inside the pump was performed. Later, and by analyzing the streamline pattern for a flowrate above the design point, we have noticed the occurrence of recirculation areas in that region. Recently, the manufacturer has made adjustments in that region and this resulted in a 5% increase in flow rate for this working point.

The pump was also analyzed working in reverse mode. A detailed analysis of the flow inside the pump, comparing both operating modes was performed. This allowed us to know the areas in which the losses are being generated. These being different in both operating modes. Actually the efficiency in reverse mode is lower than in pump mode. The care taken to treat the structural vanes in the back-rotor allowed us to analyze the behavior of the axial shaft force in direct and reverse mode. We concluded that in reverse mode the pump works with higher pressure levels, but this is not translated into axial force. Actually, the axial force is comparatively lower in turbine mode. This is beneficial because we don not need to worry about exceeding axial shaft force when changing from pump to turbine mode.

Acknowledgement

The present work was partly supported by CAST – Center for Aerospace Sciences and Technology at University of Beira Interior (Portugal).

References

[1] Efaflu, Industry - Serie NNJ - Normalized Pumps, Efaflu-Bombas e Ventiladores S.A.Povoa do Varzim, Portugal (2009).

[2] Wu Yuzhen, Huang Hao, Experimental research of pressure distribution in the casing of inducer, Journal of Thermal Science 18 (4) (2009) 301–305.

[3] R. Kawashima, M. Uno, T. Kanemoto, Approaches to stable operation of shaftless centrifugal pump, Journal of Thermal Science 18 (1) (2009) 48–53.

[4] D. Croba, J. L. Kueny, Numerical calculation of 2D unsteady flow in centrifugal pumps: impeller and volute interaction, International Journal for Numerical Methods in Fluids 22 (1996) 467–481.

[5] J. C. Páscoa, A. C.Mendes, L.M. C. Gato, R. Elder, Aerodynamic design of turbomachinery cascades using an enhanced time-marching finite volume method, Computer Modeling in Engineering & Sciences 6 (6) (2004) 537–546.

[6] J. C. Páscoa, A. C.Mendes, L.M. C. Gato, A fast iterative inverse method for turbomachinery blade design, Mechanics Research Communications 36 (5) (2009) 630–637.

[7] J. V. Voorde, J. Vierendeels, E. Dick, A force-based grid manipulator for ALE calculations in a lobe pump, Journal of Thermal Science 12 (4) (2003) 318–322.

[8] J. Li, H. Tsukamoto, A real-coded genetic algorithm applied to optimum design of a low solidity vaned diffuser for diffuser pump, Journal of Thermal Science 10 (4)

(2001) 301–308.

[9] R. A. Van den Braembussche, Flow and loss mechanisms in volutes of centrifugal pumps, in: Design and Analysis of High Speed Pumps RTO-ENAVT-143 (NATO), Rhode Saint Genese, Belgium, 2006, pp. 12.1–12.26.

[10] A. Wada, Flow structure around the intake of a vertical pump, Journal of Thermal Science 15 (2) (2006) 121–125.

[11] S. Kaewnai, M. Chamaoot, S. Wongwises, Predicting performance of radial flow type impeller of centrifugal pump using CFD, Journal of Mechanical Science and Technology 23 (2009) 1620–1627.

[12] J.-S. Kim, W.-G. Park, Optimized inverse design method for pump impeller, Mechanics Research Communications 27 (4) (2000) 465–473.

[13] T. W. Ha, A. S. Lee, A modeling of pump impeller shroud and wear-ring seal as a whole, and its application to the pump rotordynamics, Journal of Mechanical Science and Technology 12 (3) (1998) 441–450.

[14] M. Tan, S. Yuan, H. Liu, K. W. Y. Wang, Numerical research on performance prediction for centrifugal pumps, Chinese Journal of Mechanical Engineering 23 (1) (2010) 1–6.

[15] G. Kalitzin, G. Medic, G. Iaccarino, P. Durbin, Near-wall behavior of RANS turbulence models and implications for wall functions, Journal of Computational Physics 204 (2005) 265–291.

[16] J. C. Páscoa, C. M. Xisto, E. Göttlich, Performance assessment limits in transonic 3D turbine stage blade rows using a mixing-plane approach, Journal of Mechanical Science and Technology DOI: 10.1007/s12206-010-0713-9 (2010).

[17] J. González, J. M. F. Oro, K. M. Argüelles-Díaz, C. Santolaria, Flow analysis for a double suction centrifugal machine in the pump and turbine operation modes, International Journal for Numerical Methods in Fluids 61 (2008) 220–236.

[18] R. Spence, J. Amaral-Teixeira, A CFD parametric study of geometrical variations on the pressure pulsations and performance characteristics of a centrifugal pump, Computers & Fluids 38 (2009) 1243–1257.

[19] S. Saito, M. Shibata, H. Fukae, E. Outa, Computational cavitation flows at inception and light stages on an axial-flow pump blade and in a cage guided control valve, Journal of Thermal Science 16 (4) (2007) 337–345.

[20] J. González, J. Fernádez, E. Blanco, C. Santolaria, Numerical simulation of the dynamic effects due to impeller-volute interaction in a centrifugal pump, Journal of Fluids Engineering 124 (2002) 348–355.

[21] S. Derakhshan, A. Nourbakhsh, Theoretical, numerical and experimental investigation of centrifugal pumps in reverse operation, Experimental Thermal and Fluid Science 32 (2008) 1620–1627.

[22] A. Williams, N. Smith, C. Bird, M. Howard, Pumps as turbines and induction motors as generators for energy recovery in water supply systems, Water and Environment Journal, 12 (3) (1998) 175–178.